Journal of Membrane Science 612 (2020) 118429

Contents lists available at ScienceDirect

Journal of Membrane Science

journal homepage: http://www.elsevier.com/locate/memsci

Transforming polymer hollow fiber membrane modules to mixed-matrix hollow fiber membrane modules for propylene/propane separation

Sunghwan Park [a], Hae-Kwon Jeong [a,b,*]

[a] Artie McFerrin Department of Chemical Engineering, Texas A&M University, 3122 TAMU, College Station, TX, 77843-3122, United States
[b] Department of Materials Science and Engineering, Texas A&M University, 3122 TAMU, College Station, TX, 77843-3122, United States

ARTICLE INFO

Keywords:
Mixed-matrix membranes
Propylene/propane separation
Gas separation
Hollow fiber membranes
Membrane modules

ABSTRACT

Mixed-matrix membranes (MMMs) have shown promising performances for gas separation, in particular, propylene/propane separation. Their commercial applications require to fabricate MMMs in scalable forms, i.e., asymmetric mixed-matrix hollow fiber membranes (MMHFMs). Up until now, however, there have been few reports on MMHFMs due to the fundamental engineering challenges associated with current fiber spinning processes using filler-suspended dope solutions. Recently, we proposed a scalable MMM fabrication strategy, namely polymer-modification-enabled *in-situ* metal-organic framework formation (PMMOF). The PMMOF has potential to overcome some of the engineering challenges since it decouples hollow fiber spinning step and MMM formation step. Herein, we report asymmetric 6FDA-DAM (4,4′-(hexafluoroisopropylidene) diphthalic anhydride-2,4,6-trimethyl-1,3-diaminobenzene)/ZIF-8 MMHFM modules by transforming 6FDA-DAM coated hollow fiber membrane (HFM) modules using the PMMOF. The resulting asymmetric MMHFM modules showed a promising propylene/propane separation performance (i.e., propylene permeance of ~2.15 GPU and separation factor of ~23.4) without additional defect healing steps. The membranes showed stable separation performance over a period of up to 25 days and at the total feed pressures of up to 6 bar. Finally, we demonstrated MMHFM modules consisting of up to seven individual fiber strands. To the best of our knowledge, this is the first multi-strand MMHFM modules showing promising propylene/propane separation performances, thereby opening up the possibility of the commercial applications of MMMs.

1. Introduction

Membrane-based propylene/propane (C3 separation) separation is an energy-efficient alternative to conventional thermally-driven technologies such as distillation [1]. Nevertheless, the efficiency of energy saving depends largely on the separation performance of membranes [2]. The inherent separation performance limitation (i.e., trade-off between permeability and selectivity) of cost-effective and scalable polymeric membranes precludes the polymer membranes from satisfying the commercial-attractive C3 separation performance criteria (i.e., >1 Barrer of C_3H_6 permeability and >35 of C3 selectivity) [3,4]. Although polycrystalline molecular sieve membranes such as ZIF-8 membranes showed surprisingly high C3 separation performance [5–7], they are prohibitively expensive mainly due to the difficulty and complexity of synthesis among others [8]. Thus there have been great research interests in mixed-matrix membranes (MMMs) combining advantages of both processible polymer and molecular sieve membranes by dispersing a molecular sieve phase with a continuous polymer phase [9–12].

Despite the impressive advancement over decades, the majority of the reported MMMs were in flat sheet forms. Given the area-to-volume ratio, however, hollow fiber forms are much more desirable for large-scale applications [13–17]. The rarity of mixed-matrix hollow fiber membranes (MMHFMs) testifies the engineering challenges associated with spinning high-quality fibers using filler-containing dope solutions [18,19]. There have been only very few reports on MMHFMs, in particular, for C3 separation which requires much fewer defects than other light gas separations [18]. Koros and his coworkers [18] were the first to successfully demonstrate 6FDA-DAM/ZIF-8 MMHFMs with ZIF-8 loading as high as 30 wt% for C3 separation. Though pioneering, the as-spun MMHFMs showed poor C3 separation performance and the relatively high C3 separation factor (27.5) could be achieved only after multiple additional coating layers were applied [18]. It is noteworthy of mentioning that the presence of the additional coatings would increase the overall thickness of MMM skin layers. In fact, the propylene

* Corresponding author. Artie McFerrin Department of Chemical Engineering, Texas A&M University, 3122 TAMU, College Station, TX, 77843-3122, United States.
E-mail address: hjeong7@tamu.edu (H.-K. Jeong).

https://doi.org/10.1016/j.memsci.2020.118429
Received 6 May 2020; Received in revised form 8 June 2020; Accepted 21 June 2020
Available online 30 June 2020

permeance of the MMHFMs were substantially decreased after the additional coatings. It is, therefore, of critical importance to develop new MMM fabrication methodologies that enable facile and scalable formation of asymmetric MMHFMs with submicron-thick MMM skin layers exhibiting relatively high C3 separation performances without additional coating layers.

It is extremely challenging to form high-quality asymmetric MMHFMs in a scalable manner using conventional physical blending and single-step spinning methods stemming from the difficulty of controlling skin layer defects and polymer/filler interfacial structures [20–22]. Recently we proposed the polymer-modification-enabled *in-situ* metal-organic framework formation (PMMOF) as a scalable MMM fabrication method [23–25]. The PMMOF decouples polymer film deposition and MMM formation steps, thereby enabling scalable formation of MMMs with unprecedentedly thin skin layers [23,24]. Furthermore, the PMMOF is more likely to produce MMMs with less defects since MOF crystals grow *in-situ* inside polymer, effectively suppressing interfacial void formations and defective particle agglomerations [23,24]. As a proof-of-concept, we also reported fabrication of MMHFMs by the PMMOF, showing the propylene/propane separation factors of ~20 [23]. It is noted that the MMHFMs reported were premade and then assembled into a test module for gas permeation testing [23,24]. Considering the difficulty of modulation [26], it would be quite attractive if one can start with off-the-shelf polymer hollow fiber membrane (HFM) modules and transform them to MMHFM modules.

Here, we report 6FDA-DAM/ZIF-8 MMHFM modules by transforming custom-made lab-scale modules preformed with commercially-available polyethersulfone (PES) HFMs coated with 6FDA-DAM using the PMMOF process. Single-strand 6FDA-DAM/ZIF-8 MMHFM modules were fully characterized using a battery of tools. The C3 separation performances of the single-strand MMHFM modules were measured and compared with the previously reported various types of HFMs including MMHFMs. The stability of the individual membrane strands was also investigated with respect to aging and plasticization. Finally, we demonstrated and tested the first MMHFM modules consisting of up to seven strands, exhibiting increased membrane surface area and decent C3 separation performance. To the best of our knowledge, the multi-strand MMHFM modules are the first of its kind.

2. Experimental

2.1. Materials

6FDA-DAM (4,4′-(hexafluoroisopropylidene) diphthalic anhydride-2,4,6-trimethyl-1,3-diaminobenzene, Mw: 148k, PDI: 2.14) was purchased from Akron Polymer Systems Inc. Polyethersurfone (PES) microfiltration hollow fiber membrane modules (MiniKros Sampler) were purchased from Repligen corporation. Sodium formate (HCOONa, ≥ 99%), zinc nitrate hexahydrate ($Zn(NO_3)_2{\cdot}6H_2O$, 98%), 2-methylimidazole (Hmim) ($C_4H_6N_2$, 99%), and polydimethylsiloxane (PDMS, Sylgard® 184, Dow Chemical) were obtained from Sigma-Aldrich. Methanol (CH_3OH, > 99.8%, Alfa Aesar), ethyl acetate ($C_4H_8O_2$, ≥99.5%, VWR International), and hexane (C_6H_{14}, ACS grade, VWR International) were used as solvents. All chemicals were used as-received without further purification.

2.2. Polyimide coating on porous hollow fiber supports

Individual polyethersulfone (PES) hollow fiber strands (OD: ~700 μm, ID: ~500 μm and surface pore size: ~0.2 μm) were obtained by disassembling an as-purchased PES module. The hollow fiber strands were cut into smaller strands with ~10 cm in length. To coat a thin 6FDA-DAM polyimide (PI) layer on a PES fiber strand, a PI coating solution was prepared by dissolving 4 wt% of 6FDA-DAM in ethyl acetate. The PES hollow fiber membrane was then dip-coated with the coating solution in a glove bag saturated with ethyl acetate vapor. The HFM was taken out and hanged vertically in the glove bag overnight for slow solvent evaporation. The resulting 6FDA-DAM coated PES HFM was dried under air for an hour and then further dried at 60 °C overnight in a convection oven.

2.3. Modulation of hollow fibers

PI-coated HFMs were assembled into a laboratory-scale HFM module. The module was made of 316 stainless steel tube fittings (Swagelok): one 1/4 in male union cross, four 1/4 in nuts and four 1/4 in ferrule sets. Ferrule sets were connected to 1/4 in Teflon tubing cut into 3 cm and two of them were connected to the union cross at opposite sides using nuts. 1–7 fiber strands were put into the connected fitting. Both ends of the Teflon tubing were then sealed with epoxy resin (3 M Scotch-Weld DP110 flexible temperature resistant gray epoxy) using a syringe. After curing the epoxy, each end of the epoxy sealed Teflon tubing was cut to open both ends of the HFM module. The nuts and ferrule sets were connected to the ends of the module. The module was ~10 cm long with the effective HFM length of ~6 cm. Fig. S1 presents the photographs of the prepared HFM module.

2.4. Preparation of mixed-matrix hollow fiber membranes using the PMMOF

The PMMOF proceeded with the following steps: 1) hydrolysis, 2) ion-exchange, 3) ligand treatment, and 4) imidization [23]. All of the steps proceeded by filling the solutions from the shell side of a module loaded with a PI-coated PES hollow fiber membrane. The hydrolysis of the PI-coated PES HFM was carried out in an aqueous sodium formate solution (20 mmol of sodium formate dissolved in 30 ml D.I. water) at 120 °C for 2 h. After cooling down, the HFMs were washed with water overnight at room temperature. Na ions coordinated to the hydrolyzed PI layer were then exchanged with Zn ions. The ion-exchange was performed by treating the hydrolyzed HFM in a zinc nitrate hexahydrate solution with a various zinc content (20, 40, and 60 mmol) in 30 ml of water at room temperature for 3 h. After the ion-exchange solution was drained from the HFM module, a ligand treatment solution (25 mmol of 2-methylimidazole dissolved in 30 ml methanol) was filled into the HFM module. The HFM module containing the ligand treatment solution was then placed into a convection oven pre-heated at 40 °C for 2 h. Afterwards, the module was taken out and kept at room temperature for additional 2 h. The HFM were then washed with methanol overnight at room temperature. Finally, the HFMs were dried at room temperature for an hour and then thermally imidized at 210 °C for 3 h. It is noted that when the HFM module was filled with solutions, both ends of the module were sealed with plugs.

2.5. PDMS coating on hollow fiber membranes

For the confirmation of the absence of major defects on MMHFMs, PDMS coating was applied to the HFM modules. 2 wt% solution of Sylgard® was prepared in hexane at 75 °C for 1 h with stirring. The HFM modules were filled with the PDMS solution and the modules were shaken for 5 min. The solution was drained out of the modules. Soaking HFMs with the PDMS solution was repeated 2 more times. Finally, the module was placed in a vacuum oven and the PDMS was cured at 75 °C for 2 h under vacuum.

2.6. Characterizations

Scanning electron microscope (SEM) images were taken using a JEOL JSM-7500F at 5 keV acceleration voltage and 15 mm working distance. SEM samples were prepared by freeze fracturing in liquid nitrogen followed by Pt coating with thickness of 5 nm. Transmission electron microscopy (TEM) analysis was conducted using a FEI Tecnai FE-TEM under cryogenic conditions. TEM samples were prepared by

microtoming to ~60 nm in thickness using a Leica UC7 ultramicrotome at room temperature. X-ray diffraction (XRD) patterns were taken using a Miniflex II (Rigaku) with Cu-Kα radiation (λ = 1.5406 Å) in the 2 θ range of 5–40°. Attenuated total reflectance Fourier transform infrared (ATR-FTIR) spectra were obtained using a Nicolet iS5 spectrophotometer (Thermo Scientific) equipped with iD7 ATR with a resolution of 2 cm^{-1} and 16 scans in the wavenumber range of 4000–400 cm^{-1}. Thermogravimetric analysis (TGA) was conducted using a Q50 (TA instruments) at the temperature range of 25–800 °C with the heating rate of 10 °C min^{-1} under the air flow of 60 cm^3 min^{-1}.

2.7. Gas permeation measurements

The equimolar binary C_3H_6/C_3H_8 gas separation properties of prepared HFMs were measured using the Wicke-Kallenbach technique at room temperature under atmospheric feed pressure. The feed gas was supplied at 20 cm^3 min^{-1} while the argon sweeping gas was flowed at 20 cm^3 min^{-1} on the permeate side. Steady-states were declared when the difference in the measured C_3H_6 permeance of a sample was less than 1% in a 30 min interval. Composition of the permeated gases was determined by gas chromatography (GC 7890A, Agilent) equipped with a flame ionized detector (FID) and a HP-plot Q column. C_3H_6 single gas was used to determine the effect of the feed pressure on the permeation property of HFMs. The feed pressure was controlled using a back-pressure regulator located at the end of HFM modules.

3. Results and discussion

3.1. Transforming polymer HFM modules to PI/ZIF-8 MMFHM module by the PMMOF

The PMMOF enables transformation of a polymer hollow fiber membrane (HFM) module to a mixed-matrix hollow fiber membrane (MMHFM) module [23]. To perform the PMMOF, a thin 6FDA-DAM polyimide (PI) layer was dip-coated on a commercial polyethersulfone (PES) hollow fiber membrane, several of which were then assembled into a module with both of the ends open (see Fig. 1 and S1). PES HFMs were selected as supports due to their low material cost (~20 USD/kg), mechanical [27], chemical (mostly inert to the PMMOF) [28], and thermal stability (T_g of ~220 °C) [29] as well as their compatibility with fluorinated polyimides [30]. Ethyl acetate was carefully chosen as a solvent since it dissolves 6FDA-DAM while PES HFMs were intact in ethyl acetate (Fig. S2). The PI-coated HFMs were assembled into a module by sealing both ends with epoxy (Fig. S1).

The PMMOF process involves four steps: hydrolysis, ion exchange, ligand treatment, and imidization (Fig. S3). In our previous studies [23], we demonstrated the potential of the PMMOF to transform flat polymer membranes or single polymer hollow fiber membranes into high-quality MMMs. There were, however, several processing issues that should be addressed in order to apply the PMMOF to HFM modules. One such issue has to do with properly controlling hydrolysis reaction. Hydrolysis reaction partially deimidized a PI layer to form a poly(amic acid) sodium salt (PAA-Na) layer (Fig. S3). This hydrolysis step is essential to provide environments inside polymer, enabling accommodation of MOF precursors and eventually *in-situ* MOF formation inside polymer [23,31,32]. Since the PI coating layer on a PES HFM was much thinner (~0.75 μm) than that on a flat alumina disk (~7 μm) [23], the hydrolysis under the same conditions as in our previous work (i.e., in a sodium formate solution (3.33 M) at 120 °C for 5 h) severely damaged the PI coating layer on a HFM (Fig. 2a). As such, the hydrolysis time was reduced from 5 h to less than 3 h, thereby substantially suppressing damages to the coating layer upon the hydrolysis (Fig. 2b and c). Another challenge was to ensure sufficient soaking of a zinc solution during the ion-exchange step [23,32]. Due to the nature of the module, air bubbles were trapped in the module, thereby limiting saturation of the solution. As such, air bubbles were removed by evacuating one side of the HFM module under vacuum while solutions were supplied to the other side. During the ligand treatment step where ZIF-8 forms in polymer free volume (PAA/ZIF-8) (Fig. S3) [32], the polymer HFMs were most swelled, thereby causing damages to the skin layers in the limited space of the module (Fig. S4). It was possible to alleviate these damages by maintaining the packing density of the hollow fiber module at < 30%. The last step was to thermally imidize the PAA to the PI, stabilizing the gas separation performance of the membrane (Fig. S3) [23]. During this thermal imidization step, an epoxy with high thermal resistance was used to minimize the thermal expansion and degradation of epoxy (Fig. S5).

3.2. Characterizations of PI/ZIF-8 MMFHMs by the PMMOF

FI-IR spectra were taken to monitor the chemical modifications of the PI layer by the PMMOF (see Fig. 3). As shown in the figure, there were two strong peaks of the PI at 1723 and 1356 cm^{-1} which assigned to C═O and C–N in imide ring, respectively [33]. It is noted that these peaks related to the imide ring of the PI were not overlapped with that of the PES support. However, the C–C stretching bands of the benzene rings of the PI and the PES were overlapped at 1485 cm^{-1} [33]. Since the hydrolysis reaction during the PMMOF did not affect benzene rings, the intensity of the C–C peaks of the PI and PES overlapped was preserved upon the PMMOF. As such, the C–C peak was regarded as an internal standard. The intensities of the C═O and C–N peaks were reduced relatively comparing with that of the C–C peak upon the hydrolysis. This is because the imide ring of the PI was turned into the carboxyl group of the PAA (Fig. 3). The deimidization was quantitatively evaluated based on the changes of the ratio between the intensities of the C═O and C–C peaks. As the PI turned into the PAA-Na, the ratio decreased from 2.96 to 2.43, indicating ~18% of deimidization. This was less than that of the flat membranes (~35%) [23] due to the milder hydrolysis conditions which were necessary in order to preserve the integrity of the PI skin layer. It is worthy of mentioning that the basic Hmim solution also partially deimidized the polymer (Fig. 3). The final thermal imdization step again increased the ratio, attaining 95% of imidization (i.e., 5% of deimidization) (Fig. 3).

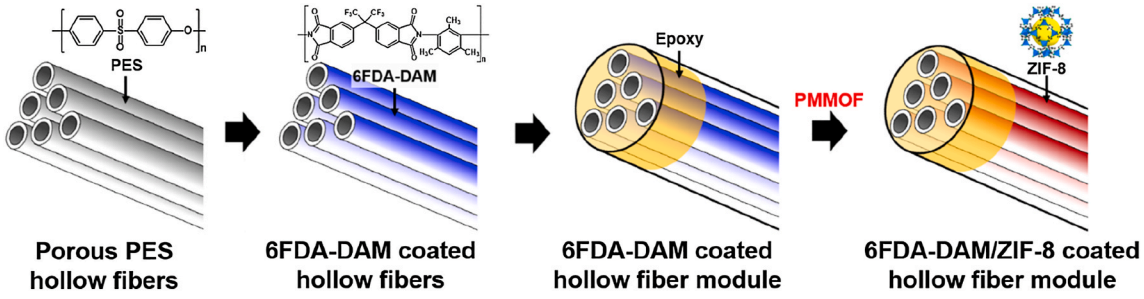

Fig. 1. Schematic illustration of evolution of commercial polymer (PES) HFMs to PI-coated polymer HFMs to a PI-coated HFM module to a PI/ZIF-8 MMHFM module.

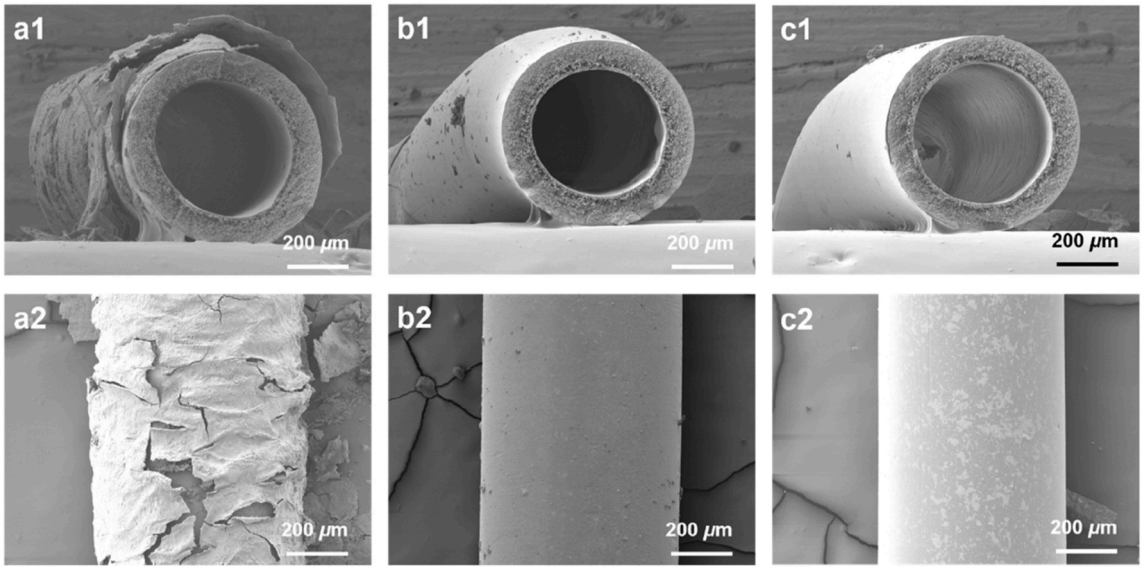

Fig. 2. SEM images of PI/ZIF-8 MMHFMs prepared under normal hydrolysis times: (a) 5 h, (b) 3 h, and (c) 2 h. (a1-c1) cross-section and (a2-c2) top view.

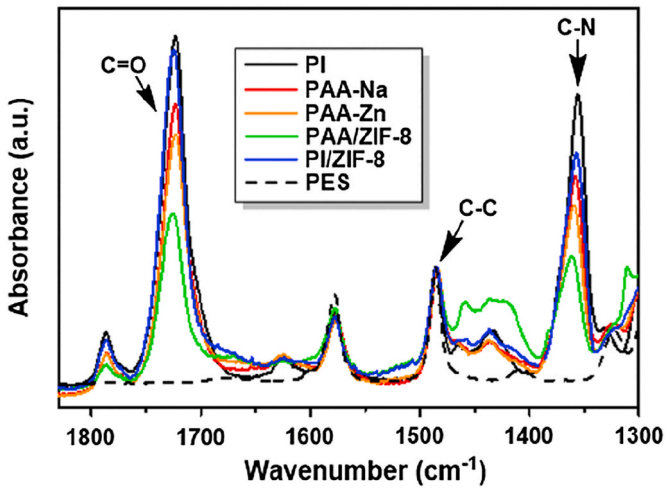

Fig. 3. Evolution of the FT-IR spectrum of a sample during the PMMOF process.

The dimensions and morphology of the HFMs were determined by SEM images. The commercial PES microfiltration HFMs used in this study possess the outer diameter of ~700 μm and the inner diameter of ~500 μm (Fig. 4a1). They were symmetrically porous with the surface pore size of ~200 nm (Fig. 4a2) [34]. When the shell sides of the PES HMFs were coated with PI, the porous surfaces of the PES HFMs were completely covered with PI coating layers of ~750 nm thickness (Fig. 4b). The thickness of the PI coating was controlled by varying the polymer concentration in a dope solution. It was found that the thickness of the skin layer was linearly correlated with the polymer concentration in a dope solution (Fig. S6). Importantly, the submicron thickness of the PI coating layer was well-preserved throughout the PMMOF steps (Fig. 4c1). There was no delamination possibly due to the proper affinity between the two polymers and the similar expansion/shrinking rates [30].

The *in-situ* formation of ZIF-8 in the polymer HFMs was investigated by XRD patterns. After the PMMOF, there appeared a strong (110) diffraction peak at 7.3° of 2θ and a relatively low intensity of (112) peak at 12.8° of 2θ along with the broad amorphous hump from polymer (Fig. S7). The peaks were well-matched with those of simulated ZIF-8 diffraction patterns, indicating the formation of ZIF-8 (Fig. S7). As shown in Fig. 4c and Fig. S8a, however, ZIF-8 particles of ~100 nm and ~200 nm in size were founded on the membrane surface as well as inside the porous support, respectively. It is noted that the ZIF-8 precursor solutions were likely percolated from the shell side of HFMs and filled in pores on the lumen side of HFMs, forming ZIF-8 crystals on the support layer. These ZIF-8 particles were removed by flowing a nitric acid solution (0.1 M) through the bore (Fig. S8b) followed by dropping the acid solution on the surface (Fig. S8c). After the sequential acid treatments, there was the notable intensity reduction of the PI/ZIF-8 MMHFM. Nevertheless, it showed the relatively strong intensity of the diffraction pattern, strongly indicating the presence of a substantial amount of *in-situ* formed ZIF-8 particles inside the skin layer (Fig. 5).

To further confirm the presence of *in-situ* formed ZIF-8 particles inside the PI layer, TEM analysis was performed. Fig. 6 presents the TEM images and the corresponding selected area electron diffraction (SAED) patterns. It is noted that the TEM analysis was carried out on the acid-treated sample to exclude ZIF-8 grown outside the polymer layer. The SAED pattern (Fig. 6a) was well-matched with that of ZIF-8 in literatures [35], confirming that the darker regions in the TEM images (Fig. 6b and c) were randomly oriented *in-situ* grown ZIF-8 crystals inside the PI layer. As shown in Fig. 6b and c, the *in-situ* formed ZIF-8 in the skin layer represented unique morphologies as observed in our previous reports [23,24]. ZIF-8 agglomerates show ring-like and rod-like shapes, likely resulting from the confined growth of ZIF-8 inside the polymer free volume. When the PI is hydrolyzed (i.e., deimidized), the free volume of the resulting polymer (i.e., PAA-Na) is drastically increased, providing enlarged spaces for ZIF-8 formation [23]. Further studies are required to understand the *in-situ* formation of uniquely-shaped ZIF-8 particles inside polymer by the PMMOF.

The maximum loading percentages of ZIF-8 fillers in the polymer were estimated to 14.5, 19.6, and 29.6 wt% (Table S1). In our previous work [23], a similar observation was made in that ZIF-8 content in a polymer was increased as the zinc concentration in ion exchange solutions increased. The percentages of ZIF-8 loading were calculated based on the contents of ZnO residue formed upon thermal decomposition under air flow (Fig. S9). The detailed explanation for the loading calculation in PI/ZIF-8 MMFHMs is represented in the Supporting Information. For clarification, PI/ZIF-8 MMHFM samples with different ZIF-8 loading were named with loading (wt%) in bracket (i. e., PI/ZIF-8 (15) is a PI/ZIF-8 MMFHM with 15 wt% loading).

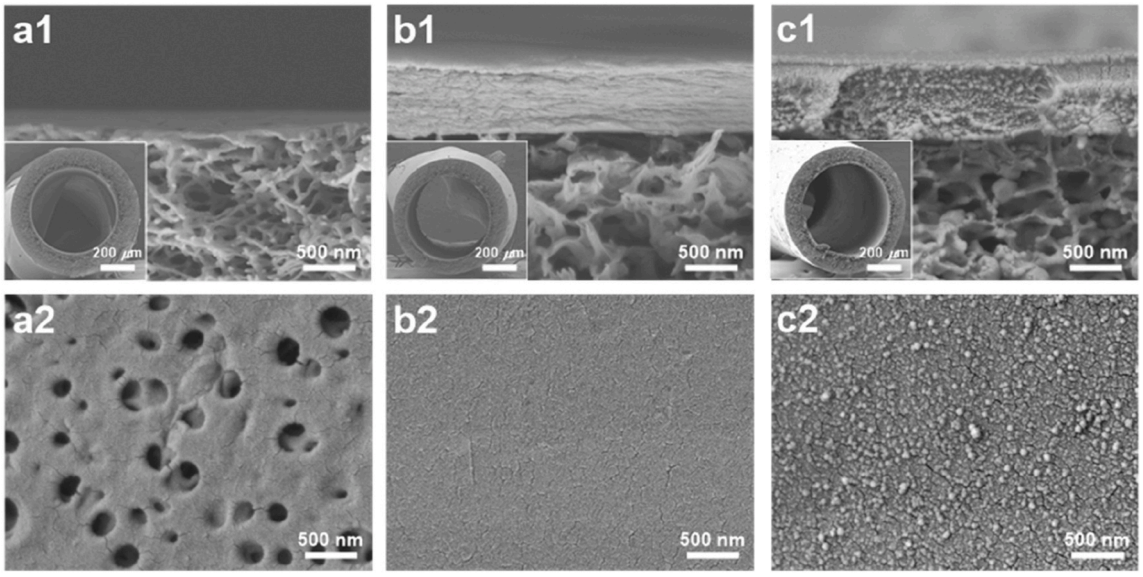

Fig. 4. SEM images of the shell sides of (a) pristine PES HFM, (b) PI-coated HFM, and (c) PI/ZIF-8 MMHFM: cross-sectional view (a1, b1, and c1) and top view (a2, b2, and c2). Inset images in a1-c1 represent low magnification images of cross-sections of HFMs.

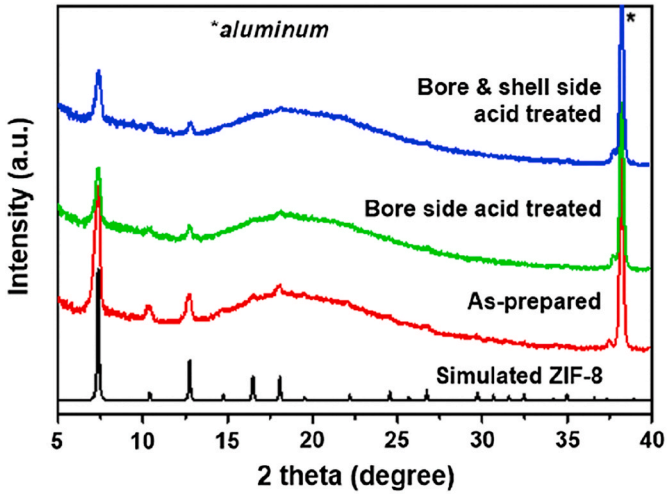

Fig. 5. XRD patterns of as-prepared PI/ZIF-8 MMHFMs along with PI/ZIF-8 MMHFMs acid-treated on bore side and acid-treated both bore and shell sides with a nitric acid solution.

3.3. Gas permeation of PI/ZIF-8 MMFHMs by the PMMOF

3.3.1. C_3H_6/C_3H_8 separation performance

The C3 separation performances of the PI/ZIF-8 MMHFM modules were comparable with those of the corresponding previously reported single-fiber MMHFMs [23]. For example, the C_3H_6 permeances of the PI/ZIF-8 (20) MMHFM modules were ~2.17 GPU (single fiber) and ~2.55 GPU (module) [23]. Besides, the separation factors were ~20 (single fiber) and ~19.3 (module) [23]. This strongly suggests that the PMMOF could be applied to hollow fibers whether they are in a module or individual fibers.

We investigated the effect of ZIF-8 contents on C3 separation performance. When the loading percentages of ZIF-8 in the PI/ZIF-8 MMHFMs increased, the C3 separation factor increased because of the molecular sieving effect of ZIF-8 (Fig. 7a and Table S2) [36]. ZIF-8 loading had a little effect on the C_3H_6 permeances of the PI/ZIF-8 MMHFMs. It is likely due to the interplay between the permeability increase by microporous ZIF-8 [9,11] and the permeability decrease by the reduced free volume of polymer upon the PMMOF process [23]. Upon the PMMOF, the C_3H_6 permeance was significantly reduced (about five-fold) (Fig. 7a and Table S2). This noticeable permeance reduction was likely because of the polymer densification upon the PMMOF [23, 37]. Nevertheless, the separation factor of the PI/ZIF-8 MMHFMs was significantly increased at the higher ZIF-8 loadings.

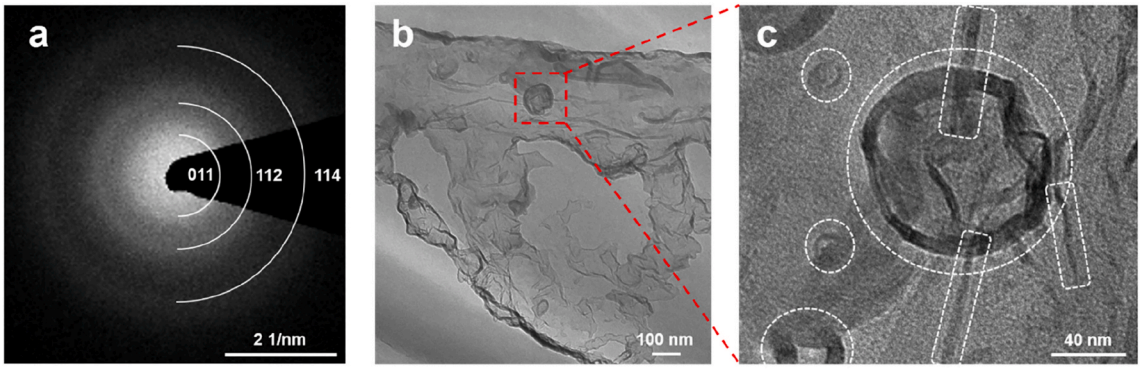

Fig. 6. TEM analysis of *in-situ* grown ZIF-8 in the PI skin layer: (a) selected area electron diffraction (SAED) pattern, (b) low magnification TEM image, (c) high magnification TEM image. Note that the SAED was taken from the sample area of (c).

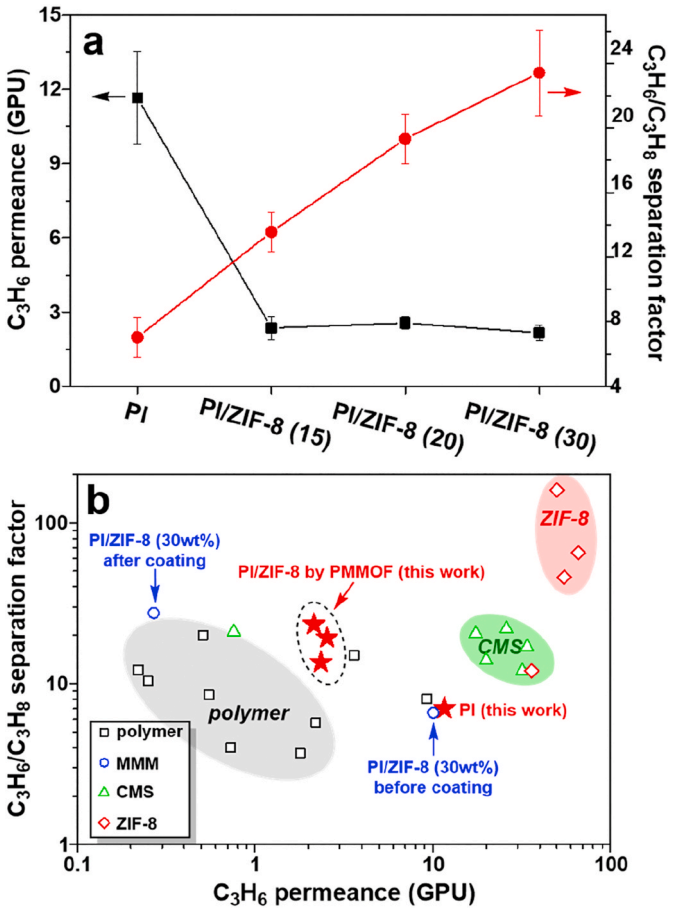

Fig. 7. (a) Effect of ZIF-8 loading on C3 separation performance and (b) C_3H_6 permeance and C3 separation factor of single-strand PI/ZIF-8 MMHFM modules in comparison with those of the HFMs previously reported [6,18,38–48].

The C3 separation performances of the single-strand PI/ZIF-8 MMHFM modules were compared with previously reported other hollow fiber membranes including polymer [38–42], CMS [43–45], ZIF-8 [6,46–48], and PI/ZIF-8 MMHFMs prepared by conventional blending methods [18]. Despite the potential of MMHFMs, to best of our knowledge, there has been only one report on MMHFMs for C3 separation so far. Even though the PI/ZIF-8 MMHFMs prepared by a blending method showed C3 separation capability, the separation factor of the as-spun MMHFMs was lower than that of the polymer HFMs due to defects (Fig. 7b) [18]. Therefore, additional coating steps were necessary to improve the separation factor, significantly sacrificing propylene permeance (Fig. 7b). The defects on MMHFMs were generally formed upon spinning process due to the complicated parameters associated with spinning a filler suspended dope solution [49]. Unlike the PI/ZIF-8 MMHFMs made by conventional blending, the MMHFMs by the PMMOF showed more improved C3 separation performances even without additional coatings (Fig. 7b). When additional PDMS coating was applied to the PI/ZIF-8 MMHFMs prepared by the PMMOF, there were no further improvements of the C3 separation factor, indicating the absence of major defects. It is surmised that decoupling of spinning step and MMM formation step in the PMMOF effectively suppressed defect formations.

3.3.2. *Stability of the C_3H_6/C_3H_8 separation performances*

It is of great practical interest to investigate the time-dependent and pressure-dependent separation performances [50,51]. First, the time-dependent separation performances of the PI HFM and PI/ZIF-8 (30) MMHFM were monitored for 25 days with 5 days intervals. A PI HFM showed gradual decrease in the C_3H_6 permeance during the period of the test (Fig. 8a), which was likely due to the aging effect of the PI. Due to its inherently high fractional free volume (FFV), the PI (i.e., 6FDA-DAM) is known to be susceptible to aging, significantly affecting its long-term gas separation [51]. In a stark contrast, a PI/ZIF-8 (30) MMHFM showed unexpectedly stable C_3H_6 permeance and C3 separation factor with time (Fig. 8a). This stable performance might be attributed to the improved adhesion between PI and ZIF-8 as well as the free volume reduction by *in-situ* growth of ZIF-8 in the polymer. Similarly, MMMs without interfacial voids showed stable gas separation performances due to a partial anti-aging effect in the presence of fillers [11,52].

The stability of C3 separation performance under the high pressure is of critical importance since condensable C_3H_6 and C_3H_8 gas molecules can be strongly absorbed into the polymer, resulting in plasticization of the polymer at high pressure [53]. In this regard, the prepared HFMs were tested under the feed pressure up to 6 bar of C_3H_6 single gas. As the feed pressure increased to 2 bar, the C_3H_6 permeance of the PI HFMs decreased (Fig. 8b) which can be explained based on the dual-mode gas sorption model of glass polymer [54,55]. When the feed pressure raised over 3 bar, the C_3H_6 permeance increased (Fig. 8b) due to the plasticization. In contrast, the PI/ZIF-8 MMHFMs showed the plasticization pressure shifted above 6 bar, continuously decreasing C_3H_6 permeance over the pressure range (Fig. 8b). There were similar observations that plasticization was alleviated by fillers [56–58]. It was likely that the fillers effectively rigidified polymer chain, thereby suppressing plasticization of polymer. Furthermore, the decrease in the permeance with increasing feed pressure further supported that the prepared PI/ZIF-8 MMHFMs were defect-free [59].

3.3.3. *Scale-up of the MMHFMs by the PMMOF*

To show scalable fabrication of MMHFMs by the PMMOF, the membrane surface area of the PI/ZIF-8 (30) was increased by increasing the number of fibers packed in a HFM module (i.e., increasing the packing density). As the membrane surface area increased from 1.23 to 6.15 cm^2 (increasing packing density from 5 to 24%), the C_3H_6 flow rate increased linearly and the C3 separation factor of the PI/ZIF-8 MMHFM modules remained relatively constant (Fig. 9). When the membrane surface area further increased to 8.61 cm^2, the separation factor was sharply decreased while the C_3H_6 flow rate increased exponentially (Fig. 9). This is likely due to the facts that the fibers could be damaged by folding upon swelling in the limited space of the module. Obviously, it becomes more difficult to control defects as the membrane surface area increases. Further optimization of the PMMOF is required to suppress defect formation as number of fibers increases.

4. Conclusion

We successfully demonstrated fabrication of 6FDA-DAM/ZIF-8 MMHFM modules by transforming modules premade of commercial polymer HFMs using the PMMOF. The PMMOF enabled *in-situ* growth of ZIF-8 inside the ultrathin 6FDA-DAM skin layer (~750 nm) coated on the porous PES hollow fiber, leading to facile transformation of polymer HFM to MMHFM in a module. To the best of our knowledge, the prepared asymmetric MMHFM exhibited the thinnest MMM skin layer (i.e., ~750 nm) among the MMHFMs reported. The *in-situ* formed ZIF-8 exhibited unique morphologies likely due to confined growth in polymer free volume. Up to ~30 wt% of ZIF-8 loading in the skin layer was achieved. As the ZIF-8 loading increased, C3 separation factor increased with the small changes in C_3H_6 permeance. Compared to the MMHFM prepared by the conventional method, the MMHFM by the PMMOF showed improved C_3H_6/C_3H_8 separation performances even with no additional coatings (i.e., C_3H_6 permeance ~ 2.2 GPU of and C3 separation factor ~ 23.4). The MMHFM showed negligible aging effect on its C3 separation performance (up to 25 days) and little plasticization effect (up to 6 bar of C_3H_6). Finally, MMHFM modules containing up to 7 fiber

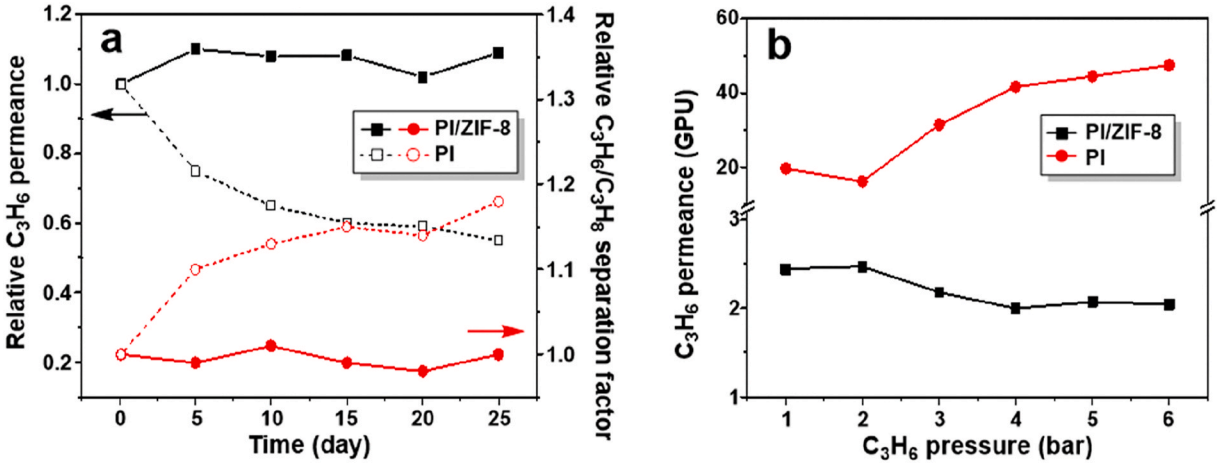

Fig. 8. C3 separation performances of a PI HFM and a PI/ZIF-8 (30) MMHFM: (a) long-term stability and (b) pressure dependent C_3H_6 permeance.

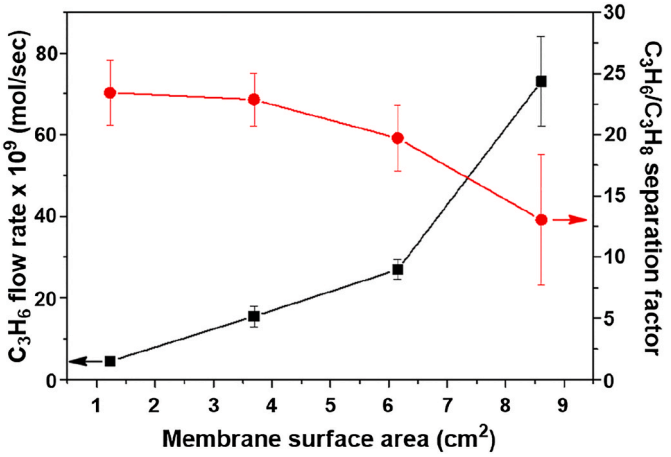

Fig. 9. C3 separation performance of PI/ZIF-8 (30) MMHFMs as a function of membrane surface area.

strands were successfully demonstrated and their C3 separation performance was measured. Although the PMMOF process needs to be further optimized for practical large-scale applications, it is expected that the multi-strand MMHFM modules presented here would be one important step toward commercial MMHFMs.

Declaration of competing interest

The authors declare that they have no known competing financial interests or personal relationships that could have appeared to influence the work reported in this paper.

Acknowledgement

H.-K.J. acknowledges the financial support from the National Science Foundation (CBET-1929596). This publication was made possible in part by NPRP grant # 12S-0209-190064 from the Qatar National Research Fund (a member of Qatar Foundation). The findings achieved herein are solely the responsibility of the authors. The National Science Foundation supported the FE-SEM acquisition under Grant DBI-0116835, the VP for Research Office, and the Texas A&M Engineering Experimental Station.

Appendix A. Supplementary data

Supplementary data to this article can be found online at https://doi.org/10.1016/j.memsci.2020.118429.

Author statement

Sunghwan Park: Conceptualization, Experiments, Data Collection/Analysis, Original draft preparation. **Hae-Kwon Jeong**: Conceptualization, Supervision, Writing- Reviewing, and Editing.

References

[1] D.S. Sholl, R.P. Lively, Seven chemical separations to change the world, Nature 532 (2016) 435–437.
[2] H.R. Amedi, M. Aghajani, Economic estimation of various membranes and distillation for propylene and propane separation, Ind. Eng. Chem. Res. 57 (2018) 4366–4376.
[3] R.L. Burns, W.J. Koros, Defining the challenges for C3H6/C3H8 separation using polymeric membranes, J. Membr. Sci. 211 (2003) 299–309.
[4] G.A.H. Craig, W. Colling, John V. Bartels, PROCESSES USING SOLID PERM-SELECTIVE MEMBRANES IN MULTIPLE GROUPS for SIMULTANEOUS RECOVERY of SPECIFIED PRODUCTS from A FLUID MIXTURE, in, US, 2004.
[5] H.T. Kwon, H.K. Jeong, A.S. Lee, H.S. An, J.S. Lee, Heteroepitaxially grown zeolitic imidazolate framework membranes with unprecedented propylene/propane separation performances, J. Am. Chem. Soc. 137 (2015) 12304–12311.
[6] K. Eum, C. Ma, A. Rownaghi, C.W. Jones, S. Nair, ZIF-8 membranes via interfacial microfluidic processing in polymeric hollow fibers: efficient propylene separation at elevated pressures, ACS Appl. Mater. Interfaces 8 (2016) 25337–25342.
[7] S. Zhou, Y.Y. Wei, L.B. Li, Y.F. Duan, Q.Q. Hou, L.L. Zhang, L.X. Ding, J. Xue, H. H. Wang, J. Caro, Paralyzed membrane: current-driven synthesis of a metal-organic framework with sharpened propene/propane separation, Sci. Adv. 4 (2018) 1393–1400.
[8] M. Tsapatsis, Toward high-throughput zeolite membranes, Science 334 (2011) 767–768.
[9] C. Zhang, Y. Dai, J.R. Johnson, O. Karvan, W.J. Koros, High performance ZIF-8/6FDA-DAM mixed matrix membrane for propylene/propane separations, J. Membr. Sci. 389 (2012) 34–42.
[10] R.J. Lin, L. Ge, H. Diao, V. Rudolph, Z.H. Zhu, Propylene/propane selective mixed matrix membranes with grape-branched MOF/CNT filler, J. Mater. Chem. 4 (2016) 6084–6090.
[11] H. An, S. Park, H.T. Kwon, H.K. Jeong, J.S. Lee, A new superior competitor for exceptional propylene/propane separations: ZIF-67 containing mixed matrix membranes, J. Membr. Sci. 526 (2017) 367–376.
[12] D.H. Liu, L. Xiang, H. Chang, K. Chen, C.Q. Wang, Y.C. Pan, Y.S. Li, Z.Y. Jiang, Rational matching between MOFs and polymers in mixed matrix membranes for propylene/propane separation, Chem. Eng. Sci. 204 (2019) 151–160.
[13] M.R.A. Hamid, H.K. Jeong, Recent advances on mixed-matrix membranes for gas separation: opportunities and engineering challenges, Kor. J. Chem. Eng. 35 (2018) 1577–1600.
[14] D. Bastani, N. Esmaeili, M. Asadollahi, Polymeric mixed matrix membranes containing zeolites as a filler for gas separation applications: a review, J. Ind. Eng. Chem. 19 (2013) 375–393.
[15] N. Jusoh, Y.F. Yeong, T.L. Chew, K.K. Lau, A.M. Shariff, Current development and challenges of mixed matrix membranes for CO2/CH4 separation, Separ. Purif. Rev. 45 (2016) 321–344.

[16] H.B. Park, J. Kamcev, L.M. Robeson, M. Elimelech, B.D. Freeman, Maximizing the right stuff: the trade-off between membrane permeability and selectivity, Science 356 (2017) 1137–1148.
[17] T.S. Chung, L.Y. Jiang, Y. Li, S. Kulprathipanja, Mixed matrix membranes (MMMs) comprising organic polymers with dispersed inorganic fillers for gas separation, Prog. Polym. Sci. 32 (2007) 483–507.
[18] C. Zhang, K. Zhang, L.R. Xu, Y. Labreche, B. Kraftschik, W.J. Koros, Highly scalable ZIF-based mixed-matrix hollow fiber membranes for advanced hydrocarbon separations, AIChE J. 60 (2014) 2625–2635.
[19] T.T. Moore, W.J. Koros, Non-ideal effects in organic-inorganic materials for gas separation membranes, J. Mol. Struct. 739 (2005) 87–98.
[20] D.T. Clausi, W.J. Koros, Formation of defect-free polyimide hollow fiber membranes for gas separations, J. Membr. Sci. 167 (2000) 79–89.
[21] A.L. Ahmad, T.A. Otitoju, B.S. Ooi, Hollow fiber (HF) membrane fabrication: a review on the effects of solution spinning conditions on morphology and performance, J. Ind. Eng. Chem. 70 (2019) 35–50.
[22] L.Y. Jiang, T.S. Chung, C. Cao, Z. Huang, S. Kulprathipanja, Fundamental understanding of nano-sized zeolite distribution in the formation of the mixed matrix single- and dual-layer asymmetric hollow fiber membranes, J. Membr. Sci. 252 (2005) 89–100.
[23] S. Park, M.R.A. Hamid, H.K. Jeong, Highly propylene-selective mixed-matrix membranes by in situ metal organic framework formation using a polymer-modification strategy, ACS Appl. Mater. Interfaces 11 (2019) 25949–25957.
[24] S. Park, H.K. Jeong, In-situ linker doping as an effective means to tune zeolitic-imidazolate framework-8 (ZIF-8) fillers in mixed-matrix membranes for propylene/propane separation, J. Membr. Sci. 596 (2020) 117689–117696.
[25] S. Park, K.Y. Cho, H.-K. Jeong, Polyimide/ZIF-7 mixed-matrix membranes: understanding the in situ confined formation of the ZIF-7 phases inside a polymer and their effects on gas separations, J. Mater. Chem. A 8 (2020) 11210–11217.
[26] D.F. Li, R. Wang, T.S. Chung, Fabrication of lab-scale hollow fiber membrane modules with high packing density, Separ. Purif. Technol. 40 (2004) 15–30.
[27] T.S. Chung, J.J. Qin, J. Gu, Effect of shear rate within the spinneret on morphology, separation performance and mechanical properties of ultrafiltration polyethersulfone hollow fiber membranes, Chem. Eng. Sci. 55 (2000) 1077–1091.
[28] N. Arahman, Mukramah Nursidik, S. Maulidayanti, A.O. Putri, The stability of Poly (ether sulfone) membranes treated in hot water and hypochlorite solution, Procedia Chem. 16 (2015) 709–715.
[29] M.C. Righetti, A. Boggioni, M. Laus, D. Antonioli, K. Sparnacci, L. Boarino, Thermal and mechanical properties of PES/PTFE composites and nanocomposites, J. Appl. Polym. Sci. 130 (2013) 3624–3633.
[30] D.F. Li, T.S. Chung, R. Wang, Y. Liu, Fabrication of fluoropolyimide/polyethersulfone (PES) dual-layer asymmetric hollow fiber membranes for gas separation, J. Membr. Sci. 198 (2002) 211–223.
[31] T. Tsuruoka, M. Kumano, K. Mantani, T. Matsuyama, A. Miyanaga, T. Ohhashi, Y. Takashima, H. Minami, T. Suzuki, K. Imagawa, K. Akamatsu, Interfacial synthetic approach for constructing metal-organic framework crystals using metal ion-doped polymer substrate, Cryst. Growth Des. 16 (2016) 2472–2476.
[32] M.R.A. Hamid, S. Park, J.S. Kim, Y.M. Lee, H.K. Jeong, In situ formation of zeolitic-imidazolate framework thin films and composites using modified polymer substrates, J. Mater. Chem. 7 (2019) 9680–9689.
[33] H.T. Kim, S.K. Kim, J.K. Park, Development of in-plane orientation in pyromellitic dianhydride-oxydianiline polyimide film on substrate during thermal imidization, Polym. J. 31 (1999) 154–159.
[34] M.M. Pendergast, E.M.V. Hoek, A review of water treatment membrane nanotechnologies, Energy Environ. Sci. 4 (2011) 1946–1971.
[35] P.B. Gai, H.J. Zhang, Y.S. Zhang, W. Liu, G.B. Zhu, X.H. Zhang, J.H. Chen, Simultaneous electrochemical detection of ascorbic acid, dopamine and uric acid based on nitrogen doped porous carbon nanopolyhedra, J. Mater. Chem. B 1 (2013) 2742–2749.
[36] C. Zhang, R.P. Lively, K. Zhang, J.R. Johnson, O. Karvan, W.J. Koros, Unexpected molecular sieving properties of zeolitic imidazolate framework-8, J. Phys. Chem. Lett. 3 (2012) 2130–2134.
[37] T.C.J. Hsu, Z.L. Liu, Solvent effect on the curing of polyimide resins, J. Appl. Polym. Sci. 46 (1992) 1821–1833.
[38] J.J. Krol, M. Boerrigter, G.H. Koops, Polyimide hollow fiber gas separation membranes: preparation and the suppression of plasticization in propane/propylene environments, J. Membr. Sci. 184 (2001) 275–286.
[39] T. Visser, A. Wessling, Auto and mutual plasticization in single and mixed gas C-3 transport through Matrimid-based hollow fiber membranes, J. Membr. Sci. 312 (2008) 84–96.
[40] A. Ito, S.T. Hwang, Permeation of propane and propylene through cellulosic polymer membranes, J. Appl. Polym. Sci. 38 (1989) 483–490.
[41] M. Yoshino, S. Nakamura, H. Kita, K. Okamoto, N. Tanihara, Y. Kusuki, Olefin/paraffin separation performance of asymmetric hollow fiber membrane of 6FDA/BPDA-DDBT copolyimide, J. Membr. Sci. 212 (2003) 13–27.
[42] K. Okamoto, M. Yoshino, K. Noborio, H. Maeda, K. Tanaka, H. Kita, Preparation of carbon molecular sieve membranes and their gas separation properties, in: Acs Sym Ser, vol. 744, 2000, pp. 314–329.
[43] L.R. Xu, M. Rungta, M.K. Brayden, M.V. Martinez, B.A. Stears, G.A. Barbay, W. J. Koros, Olefins-selective asymmetric carbon molecular sieve hollow fiber membranes for hybrid membrane-distillation processes for olefin/paraffin separations, J. Membr. Sci. 423 (2012) 314–323.
[44] K. Okamoto, S. Kawamura, M. Yoshino, H. Kita, Y. Hirayama, N. Tanihara, Y. Kusuki, Olefin/paraffin separation through carbonized membranes derived from an asymmetric polyimide hollow fiber membrane, Ind. Eng. Chem. Res. 38 (1999) 4424–4432.
[45] M. Yoshino, S. Nakamura, H. Kita, K. Okamoto, N. Tanihara, Y. Kusuki, Olefin/paraffin separation performance of carbonized membranes derived from an asymmetric hollow fiber membrane of 6FDA/BPDA-DDBT copolyimide, J. Membr. Sci. 215 (2003) 169–183.
[46] K. Eum, A. Rownaghi, D. Choi, R.R. Bhave, C.W. Jones, S. Nair, Fluidic processing of high-performance ZIF-8 membranes on polymeric hollow fibers: mechanistic insights and microstructure control, Adv. Funct. Mater. 26 (2016) 5011–5018.
[47] A.J. Brown, N.A. Brunelli, K. Eum, F. Rashidi, J.R. Johnson, W.J. Koros, C. W. Jones, S. Nair, Interfacial microfluidic processing of metal-organic framework hollow fiber membranes, Science 345 (2014) 72–75.
[48] M.J. Lee, M.R.A. Hamid, J. Lee, J.S. Kim, Y.M. Lee, H.K. Jeong, Ultrathin zeolitic-imidazolate framework ZIF-8 membranes on polymeric hollow fibers for propylene/propane separation, J. Membr. Sci. 559 (2018) 28–34.
[49] R.J. Lin, B.V. Hernandez, L. Ge, Z.H. Zhu, Metal organic framework based mixed matrix membranes: an overview on filler/polymer interfaces, J. Mater. Chem. 6 (2018) 293–312.
[50] L.L. Cui, W.L. Qiu, D.R. Paul, W.J. Koros, Responses of 6FDA-based polyimide thin membranes to CO2 exposure and physical aging as monitored by gas permeability, Polymer 52 (2011) 5528–5537.
[51] L.L. Cui, W.L. Qiu, D.R. Paul, W.J. Koros, Physical aging of 6FDA-based polyimide membranes monitored by gas permeability, Polymer 52 (2011) 3374–3380.
[52] S.J.D. Smith, C.H. Lau, J.I. Mardel, M. Kitchin, K. Konstas, B.P. Ladewig, M.R. Hill, Physical aging in glassy mixed matrix membranes; tuning particle interaction for mechanically robust nanocomposite films, J. Mater. Chem. 4 (2016) 10627–10634.
[53] S. Velioglu, M.G. Ahunbay, S.B. Tantekin-Ersolmaz, Propylene/propane plasticization in polyimide membranes, J. Membr. Sci. 501 (2016) 179–190.
[54] D.R. Paul, Gas sorption and transport in glassy-polymers, Ber. Bunsengesellschaft Phys. Chem. 83 (1979) 294–302.
[55] V. Stannett, The transport of gases in synthetic polymeric membranes — an historic perspective, J. Membr. Sci. 3 (1978) 97–115.
[56] S. Shahid, K. Nijmeijer, Performance and plasticization behavior of polymer-MOF membranes for gas separation at elevated pressures, J. Membr. Sci. 470 (2014) 166–177.
[57] J. Yu, C.Q. Wang, L. Xiang, Y.Z. Xu, Y.C. Pan, Enhanced C3H6/C3H8 separation performance in poly(vinyl acetate) membrane blended with ZIF-8 nanocrystals, Chem. Eng. Sci. 179 (2018) 1–12.
[58] J.E. Bachman, Z.P. Smith, T. Li, T. Xu, J.R. Long, Enhanced ethylene separation and plasticization resistance in polymer membranes incorporating metal-organic framework nanocrystals, Nat. Mater. 15 (2016) 845–851.
[59] M.R. Kosuri, W.J. Koros, Defect-free asymmetric hollow fiber membranes from Torlon®, a polyamide–imide polymer, for high-pressure CO2 separations, J. Membr. Sci. 320 (2008) 65–72.